The Dynamic Interfacial Oxygen Potential between Iron-Carbon Droplets and Oxidizing Slag

Kezhuan Gu, Neslihan Dogan and Kenneth S. Coley

McMaster Steel Research Centre
Department of Materials Science and Engineering
McMaster University
1280 Main Street West, State, Hamilton, Ontario, Canada, L8S 4L7
Email: guk3@mcmaster.ca and coleyk@mcmaster.ca

Keywords: Interfacial Oxygen Potential, Oxygen Transfer, Phosphorus Reversion

ABSTRACT

The dynamic nature of the interfacial oxygen potential during dephosphorization was investigated based on the concept that P_{O_2} at the interface between slag and liquid metal is determined by the balance between oxygen supply from reducible oxides in the slag and oxygen consumption by alloying elements in the metal. Combining this approach with the knowledge that at the phosphorus reversion point the interfacial oxygen potential can be determined from the bulk phosphorus partition ratio, the mass transfer coefficient for FeO, k_{FeO},was determined for different slags and found to increase with increasing FeO content. In foamy slags k_{FeO} was found to be a linear function of slag liquid fraction. Equating the mass transfer rate of FeO in the slag with decarburization rate, the dynamic interfacial oxygen potential was calculated over the course of the reaction and its effect on the rate determining step for dephosphorization was evaluated.

I. INTRODUCTION

It is well known that the oxygen potential at the interface between "Fe_tO" containing slag and liquid iron is an important process parameter, which affects the driving force for refining reactions such as desulphurization and dephosphorization. However, since direct measurement of interfacial oxygen potential is not feasible, there is often no way to define this important parameter quantitatively. Several workers have addressed the problem of interfacial oxygen potential employing kinetic data [1-4]. Ohguchi *et al.* [1] employed a coupled reaction model to study simultaneous dephosphorization and desulphurization between molten pig iron and slag containing Fe_2O_3. They found that the interfacial oxygen activity increased firstly as the silicon transfer rate decreased, and then decreased again with the progress of the reactions. Wei *et al.* [2] who investigated reactions between iron oxide bearing slag and molten iron with high carbon, proposed that the interfacial oxygen potential is defined by the balance of the rate of oxygen supply by FeO in the slag and consumption by carbon in the metal. They further estimated $P^i{}_{O_2}$ based on the assumption that equilibrium with respect to phosphorus was established in the slag-metal system at the phosphorus reversion point, and used this to show that $P^i{}_{O_2}$ increased with the ratio of ferric

iron to total iron in the bulk slag and with the partial pressure of oxygen in the atmosphere. Using a similar approach, Monaghan *et al*. [3] found that the interfacial oxygen potential was controlled primarily by Fe-FeO equilibrium but did not find a significant dependency on the Fe^{3+}/Fe^{2+} ratio in the slag. Based on the study of simultaneous reactions between iron-carbon alloys and slags containing different content of FeO and MnO, Shibata *et al.* [4] calculated that the interfacial oxygen activity for slags with high FeO content was approximately one order of magnitude higher than those with an equivalent content of MnO.

Recent work by the authors [5] highlighted that for Fe-C droplets reacting with slag, the rate determining step and rate of dephosphorization can be changed dramatically by changes in interfacial oxygen potential during reaction. This work also showed that the phosphorus partition ratio at the reversion point decreased with increasing carbon oxidation rate. [2, 4-5] This latter result is qualitatively consistent with the findings of Wei *et al*. and to some extent with Shibata *et al*. and Monaghan *et al*. Given the importance of interfacial oxygen potential to refining, the current work seeks to offer a more detailed analysis of the authors' findings from dephosphorization of iron-carbon droplets and to offer comparison with previous studies under a range of reaction conditions. Experimental data from the authors' previous work is summarized in Section III and analysed using the concept employed by Wei *et al*. [2] to provide a detailed analysis of the dynamic interfacial oxygen potential and of oxygen (FeO) transport in foamy slags. The results of this analysis are compared with similar analysis of the data of previous workers under a range of reaction conditions and finally a method to calculate the interfacial oxygen potential is used to elucidate its effect on dephosphorization kinetics.

II. EXPERIMENTAL PROCEDURE

The primary experimental data presented in the current study are taken from a recent publication by the authors. [5] For the convenience of the reader, a brief description of the experimental procedure is repeated here. A resistance heated vertical tube furnace with an 80mm diameter alumina working tube was used. The furnace was equipped with, X-ray imaging to observe the swelling of droplets in-situ, and a pressure transducer to measure gas evolution using the constant volume pressure increase technique (CVPI). Experiments were done at 1853K (1580ºC). 25g of slag, 32wt pctCaO-35wt pctSiO2-17wt pctAl2O3-16wt pctFeO, was placed in a 45 mm diameter alumina crucible located in the hot zone of the furnace and was melted under an argon atmosphere. The Fe-C-P-S droplet, 2.62wt pctC-0.088wt pctP-(0.007 to 0.021wt pct)S, was dropped into the molten slag via a small hole at the bottom of a closed end alumina tube, thus ensuring the droplet was molten before entering the slag. Samples were quenched at different reaction times and taken for chemical analysis of phosphorous in the metal droplet using Inductively Coupled Plasma.

III. RESULTS

A. Decarburization and Dephosphorization of Bloated Droplets

Decarburization and dephosphorization data from our previous work [5] for the reaction at 1853K (1580°C) between slag and iron droplets with sulfur contents from 0.007 and 0.021wt pct are summarized in Figures 1 and 2.

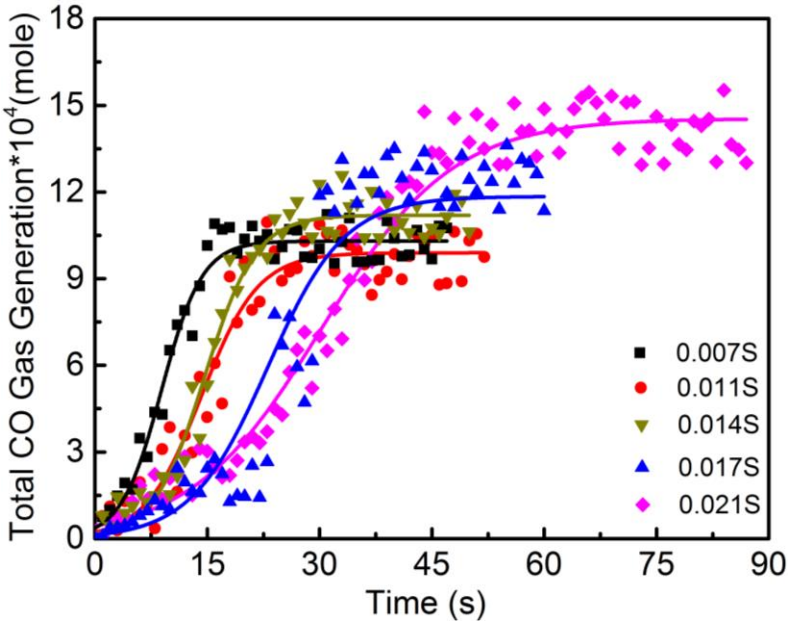

Fig. 1—CO gas generation with time for droplets containing different sulfur content.

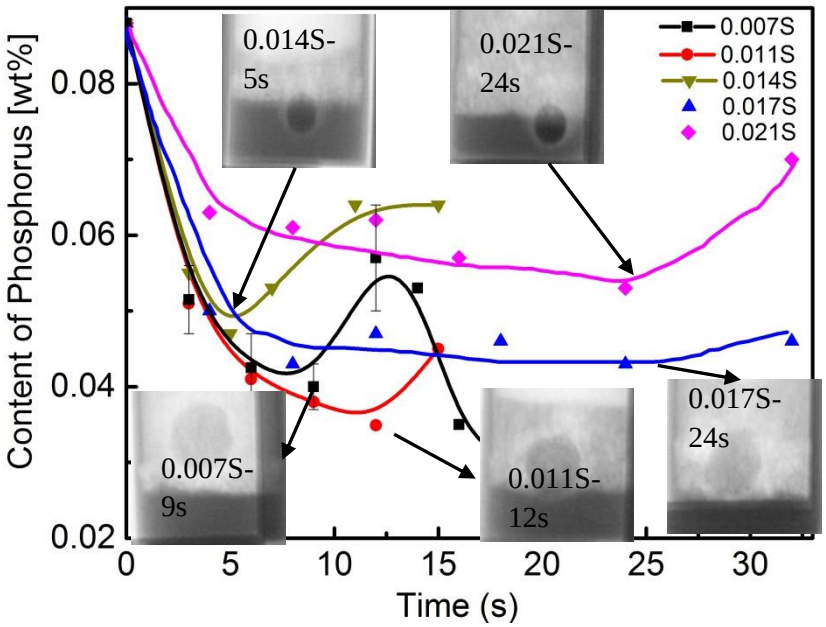

Fig. 2—Change of [%P] with time for droplets containing different sulfur content.

From Figure 1, it is possible to know the decarburization rate at any given time which can be used in analysis of the dynamic interfacial oxygen potential. During decarburization carbon monoxide caused droplets to swell (bloating behaviour) and also caused slag foaming, resulting in a layer of foamy slag sitting on top of a thinner layer of dense slag. The greater buoyancy of the bloated

droplets caused them to float into the foamy slag and then, as bloating subsided, to sink back into the dense slag. In Figure 2, all droplets exhibited some reversion due to FeO depletion and a decrease in the rate of oxygen supply. In the case of the 0.007wt pctS droplet a re-initiation of dephosphorization subsequent to reversion was observed. This can be explained if one considers that reversion occurred in the foamy slag, which was readily depleted of FeO because of its low liquid volume. The droplet then returned to the dense slag where there was a higher concentration of FeO and the dephosphorization commenced again. The decarburization and dephosphorization behavior has been discussed in detail in our previous work. [5] In the current work the phosphorus partition ratio at the reversion point will be used, in conjunction with the decarburization data, to evaluate the dynamic interfacial oxygen potential. Images of droplets in the slag at the point of reversion are also shown in Figure 2 for various sulfur contents. This figure shows that for droplets with 0.007, 0.011 and 0.017wt pctS, the reversion occurred when metal droplets entered the foamy slag; while for droplets with 0.014wt pctS the reversion took place when the droplet was in transition between the dense and foamy slag. Figure 2 also shows that droplets with 0.021wt pctS experienced reversion when sitting between dense slag and foamy slag.

Figure 3 shows that once the droplet falls into the slag, a gas halo is formed around it and slag starts to foam at the top of dense slag. After few seconds of incubation time, the droplet swells and floats up to the foaming slag due to CO nucleation inside the metal droplet. The mechanism of droplet swelling has been discussed in detail in a number of recent studies. [6-7]

Inspection of the recorded X-ray videos revealed that droplets with 0.014S and 0.021 wt pctS, were sitting between dense slag and foamy slag for a while (ranged between 6s and 18s) before completely entering the foamy slag. This is shown by the series of X-ray images in Figure 3. Combining Figure 1 and 3, it is possible to have a better understanding of the three types of phosphorus reversion behavior shown in Figure 2, *i.e.*, reversion in foamy slag (droplets with 0.007 and 0.011wt pctS), droplets in transition but primarily in dense slag (0.014wt pctS) and between dense slag and foamy slag (droplets with 0.021wt pctS). For droplets with 0.007wt pctS, the reversion occurred entirely in the foamy slag with a low rate of transport of FeO. However, reversion in the dense slag for droplets containing 0.014wt pctS was probably caused by the high rate of decarburization, causing a low interfacial oxygen potential even at higher rates of oxygen supply. Despite the low rate of decarburization, if one considers the longer period spent between foamy slag and dense slag, droplets with 0.021wt pctS exhibited a phosphorus reversion because the lower mass transfer coefficient of FeO in the foamy slag as shown in Table I.

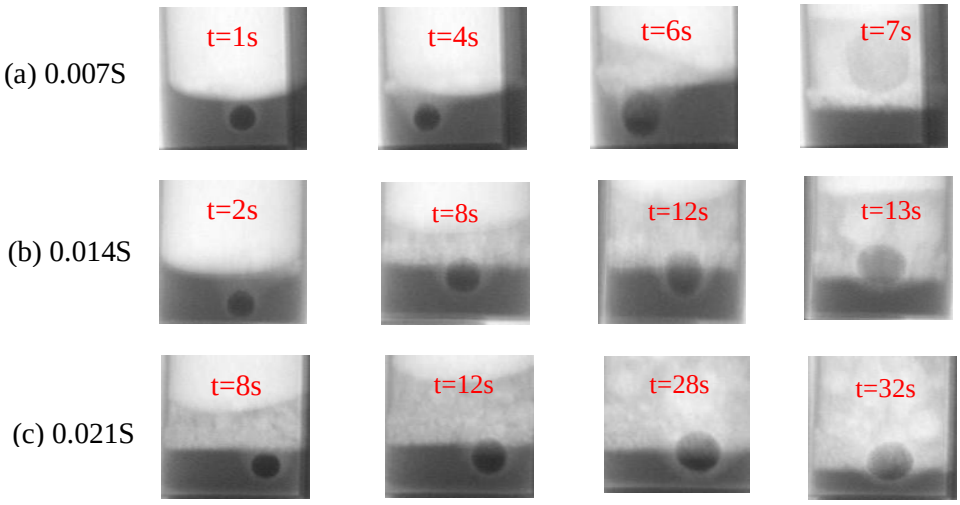

Fig. 3—Behavior of droplets before fully entering the foamy slag: (a)0.007S, (b)0.014S and (c)0.021S.

B. Mass Transfer Coefficient of FeO and Dynamic Interfacial Oxygen Potential

The interfacial oxygen potential is dictated by the balance between supply rate of FeO to the interface and the oxygen consumption by the formation of CO and P_2O_5. However, as the consumption of oxygen by phosphorous is negligible compared with that by carbon, at steady state this balance can be expressed as Eq. [1]:

$$k_{FeO}\left(C_{FeO}^{b} - C_{FeO}^{i}\right) = \frac{1}{A}\frac{dn_{CO}}{dt} \quad [1]$$

Here, $\frac{dn_{CO}}{dt}$ is the CO generation rate (mol/s), C_{FeO} is the concentration of FeO, A is the surface area of the droplet, k_{FeO} describes oxygen transport in the slag conceptually defined as the mass transfer coefficient for FeO, and superscripts b and i indicate bulk and interfacial values respectively. C_{FeO}^{i} may be expressed in terms of activity of oxygen at the interface and C_{FeO}^{b} expressed as a function of the initial value C_{FeO}^{o} modified by the amount reduced (dn_{FeO}). If one makes these substitutions and further recognizes that dn_{FeO} is equivalent to the amount of CO generated (dn_{CO}), one may rearrange Eq. 1 to obtain (detailed derivation of Eq. [2] from Eq. [1] is shown in the Appendix):

$$P_{O2}^{i} = \left[\frac{\gamma_{FeO}K_{Fe}}{C_s * a_{Fe}^{i} * K_O}\left(C_{FeO}^{o} - \frac{1}{V_S}\int_{n_{CO},t=0}^{n_{CO},t=t} dn_{CO} - \frac{1}{A}\frac{1}{k_{FeO}}\frac{dn_{CO}}{dt}\right)\right]^2 \quad [2]$$

where K_{Fe} and K_O are the equilibrium constants for FeO dissociation and oxygen dissolution in iron; γ_{FeO} is the activity coefficient for FeO in the slag, C_s is the overall molar density of the slag, C_{FeO}^{o} is molar concentration of FeO in the slag and V_S is the volume of slag, which could be volume of dense slag or foamy slag depending on the movement of droplet.

According to Eq. [2], the interfacial oxygen potential can be easily calculated by knowing k_{FeO} in the slag. Equally if knowing the interfacial oxygen potential and the decarburization rate, the k_{FeO}

can be determined. In the current work the interfacial oxygen potential $P^i{}_{O_2}$ was calculated at the point of phosphorous reversion via Eq. [3]:

$$L_P = \frac{(\%P)_i}{[\%P]_i} = \frac{C_{PO_4^{3-}} P_{O_2}^{i\ 5/4} f_P M_P}{K_P M_{PO_4^{3-}}} \quad [3]$$

where $C_{PO_4^{3-}}$ is the phosphate capacity of the slag, f_P is the Henrian activity coefficient for phosphorus in the metal, M_P and $M_{PO_4^{3-}}$ are the molar mass of phosphorus and phosphate respectively, K_P is the equilibrium constant for the dissolution of phosphorus gas in steel. $C_{PO_4^{3-}}$ was determined based on the following correlation: [8]

$$\log C_{PO_4^{3-}} = 17.55\,\Lambda + \frac{51670}{T} - 21.867 \quad [4]$$

where Λ is the theoretical optical basicity of slag.

As mentioned above, at the point of phosphorus reversion, the system is instantaneously in equilibrium with respect to phosphorus while interfacial oxygen potential continues to change via the interplay between oxygen supply and consumption represented by Eq. [2]. Therefore at the reversion point the bulk concentrations of phosphorus can be used to calculate L_P and thereby determine the interfacial oxygen potential. One can then calculate k_{FeO} by substituting $P^i{}_{O_2}$ into Eq. [2].

The measured phosphorus partition coefficient, the calculated interfacial oxygen potential and mass transfer coefficient of FeO are shown in Table I. The void fraction of foamy slag at the time where reversion occurred was calculated by comparing the heights of the dense and foamy slag with that of the initial unfoamed slag and is also shown in Table I. For droplets situated between the foamy slag and dense slag at the point of reversion (0.014 and 0.021wt pctS), an average value for the slag liquid fraction was calculated based on the fraction of the surface exposed to each type of slag.

Table I: Calculated Results for Different Metal Droplets

Sulfur content /(wt pct)	$L_P \times 10^2$	$P^i{}_{O2}$ /(atm)	$k_{FeO} \times 10^3$/(cm/s)	Liquid slag fraction	Void fraction
0.007	4.8	5.52E-12	1.44	0.10±0.007	0.90±0.007
0.011	6.1	6.65E-12	1.85	0.20±0.006	0.80±0.006
0.014	3.5	4.28E-12	10.1	0.92±0.020*	0.85±0.008
0.017	4.2	4.95E-12	2.24	0.12±0.006	0.88±0.006
0.021	2.6	3.42E-12	4.87	0.61±0.006*	0.80±0.008

*These values of liquid fraction represent a weighted average of foamy and dense slag in proportion to their contact with the droplet

Table I shows that although the slag composition was the same, the mass transfer coefficient of FeO in the slag appears to vary with sulfur content of the droplet. This observation may be understood if one recognizes that the degree to which the slag is foamed will influence the mass transfer coefficient. The mass transfer coefficient of FeO has been determined at the point of reversion and at that point the droplet may be situated in the dense slag, in the foamy slag or a combination thereof. In addition the degree to which the slag is foamed will depend on the CO generation rate. Therefore, as the CO generation rate is strongly affected by sulfur, it is not surprising that different mass transfer coefficients for FeO were determined for experiments with different metal sulfur contents. Table I also shows that in the current work higher mass transfer coefficients were determined for slags with higher liquid fractions.

IV. DISCUSSION

A. Mass Transfer of FeO in the Slag

The k_{FeO} determined for each case in Table I was plotted against the liquid fraction of slag in Figure 4 (detailed calculation of the liquid fraction of the slag is shown in the Appendix). It shows that a linear relationship exists between k_{FeO} and the fraction of liquid slag. This result is to be expected if one considers the pathway for mass transfer to be through the liquid, the cross sectional area of the path is dramatically reduced by the presence of bubbles. Because of that, the mass transfer coefficient of FeO for foamy slag (1.44×10^{-3}cm/s) is almost one tenth of the value for dense slag (10×10^{-3}cm/s). These values are of the same order as values reported by other workers *i.e.*, between 10^{-2} to 10^{-3}cm/s. [2, 4-5, 9-12]

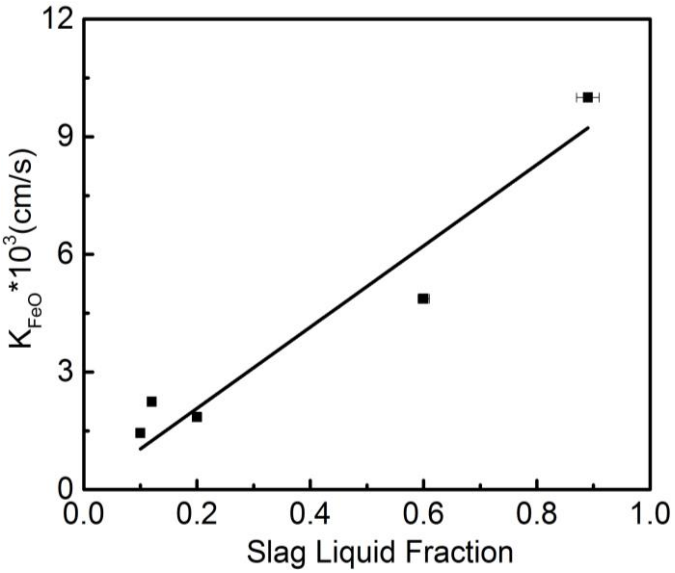

Fig. 4—k_{FeO} as a function of the liquid fraction of slag.

Shibata *et al.* [2] and Wei *et al.* [4] have conducted similar analysis of the dynamic interfacial oxygen potential but have employed a coupled reaction model fitting all fluxes over the duration of the reaction. In their case the mass transfer coefficient for all elements in the slag was assumed to be

equal. In order to compare the approaches, k_s values from these studies are shown in Table II along with k_{FeO} calculated from their data using the current approach. The experimental conditions employed in the work of Shibata *et al*. and Wei *et al*. are given in the Appendix along with the method used to calculate k_{FeO}. Calculated slag viscosity for each slag is also presented in Table II, determined using Factsage 6.4™ employing the Melts database.

Table II: Calculated k_{FeO} for Different Researchers' Work

Investigator	T/(K(°C))	Fe_tO/(wt pct)	η /poise	V_g^s/(cm/s)	$k_s \times 10^3$(cm/s)	$k_{FeO} \times 10^3$(cm/s)
Wei *et al*.	1573(1300)	15	0.86	0.11	3	1.37
Wei *et al*.	1573(1300)	15	0.86	0.10	3	2.09
Shibata *et al*.	1723(1450)	0	0.59	0.17	5	0.87
Shibata *et al*.	1723(1450)	5.4	0.41	0.22	6	0.88
Shibata *et al*.	1773(1500)	4.5	0.78	0.06	16.7	1.11
Shibata *et al*.	1773(1500)	29.7	0.61	0.60	13.3	15.1
Molloseau and Fruehan	1713 (1440)	10	1.51	0.06		1.3
Molloseau and Fruehan	1713 (1440)	20	1.02	0.4		3.8
Monaghan *et al*.	1603(1330)	38.10	0.80		3.6	
Monaghan *et al*.	1603(1330)	47.62	0.58		10	
Monaghan *et al*.	1603(1330)	57.14	0.42		28	
Monaghan *et al*.	1603(1330)	66.67	0.30		99	
This study	1853(1580)	16	1.49	0.30~0.40		1.0~10

By studying the decarburization behavior between Fe-C-S droplets and CaO-SiO_2-MgO-FeO slags, Molloseau and Fruehan [9] also determined k_{FeO} in the slag using two different methods, *i.e.*, fitting experimental data by assuming liquid phase mass transfer was the rate controlling step, and by calculation based on penetration theory. The determined k_{FeO} values for slag containing 10 and 20wt pct FeO were 1.3×10^{-3} and 3.8×10^{-3}cm/s, respectively. While the values calculated from penetration model were 4.8×10^{-3} and 1.3×10^{-2} cm/s. These workers proposed that the difference obtained from these two approaches was due to the uncertainty of average diameter of CO bubbles formed during the reaction. The experimental k_{FeO} values from Molloseau and Fruehan1.3×10^{-3} and 3.8×10^{-3}cm/s are used in the current work for slags containing 10 and 20wt pct FeO. These have been included in Table II.

By fitting dephosphorization kinetic data, Monaghan *et al*. [3] also estimated the mass transfer coefficient of phosphorous in the slag k_S for very high iron oxide slag (>35wt pct). Based on our calculations, for slag containing high iron oxide (>15wt pct) the determined values of k_{FeO} are close to a general value of k_S for all species reported by Wei *et al*. [2] (15wt pct) and Shibata *et al*.

[4] (29.7wt pct) as shown in Table II. Therefore, it has been assumed for the current discussion that the values of k_s determined in the case of Monaghan *et al*. represent a reasonable estimate of k_{FeO}.

For comparison of the mass transfer coefficients from other studies with those determined in the present work, it is important to know the slag void fraction. In order to estimate the void fraction of the slags in the work of Shibata *et al*. [4] and Wei *et al*. [2], the superficial gas velocities were calculated using decarburization data. In the case of Molloseau and Fruehan, the CO gas generation rate was employed to calculate the superficial gas velocities. Laboratory studies, where superficial gas velocity is lower than 10 cm/s, typically report void fractions of foaming slag between 0.8 and 0.9. [13-14] Therefore, for the slags with total iron less than 20wt pct it is reasonable to assume that a void fraction is between 0.8 and 0.9. However, in the cases of higher total iron oxide content (>29.7wt pct) the void fraction is expected to be lower; according to Jung and Fruehan [15], the foaming index is dramatically decreased with increasing of FeO in the slag.

Mass transfer coefficients from a range of studies have been presented in Table II. These values were determined in a number of different ways. In the current work they have been determined specifically for FeO at the point of reversion of phosphorous. Molloseau and Fruehan employed a different method but also determined k_{FeO}. In the work of Wei *et al*. [2] and Shibata *et al*. [4] k_s was determined by fitting data for the transport of all species in the slag over the entire reaction time. This approach has the advantage of including a larger data set in the calculation but may introduce errors by assuming all species have the same mass transfer coefficient. Monaghan *et al*. [3] determined the mass transfer coefficient for phosphorous in the slag. The values of k_{FeO} presented in Table II attributed to Shibata *et al.* and Wei *et al.*, were determined as part of the present work from the original data using our approach. The values for k_s were as determined by these workers. The value of k_{FeO} from the study of Molloseau and Fruehan [9] was taken directly from their work. In the absence of the additional data, the value of k_s determined by Monaghan *et al*. [3] is assumed to be equivalent to k_{FeO} which is considered reasonable because the mass transfer coefficients for different species seem to converge for high iron oxide slags. The data for mass transfer coefficients presented in Table II are plotted along with data from the current study against the FeO content of the slag in Figures 5(a) and (b) respectively for low and high liquid fraction slags. The calculated viscosities in the study of Shibata *et al*. [4] (29.7wt pct FeO) and the study of Monaghan *et al*. (>40wt pct FeO) are less than 0.61 poise, which is much lower compared to other cases therefore the liquid fraction for these slags would be expected to be much higher. Therefore we have compared the k_{FeO} data for droplets with 0.014 and 0.021wt pctS in current study, *i.e.* those for which the slag had a high liquid fraction with cases from Shibata *et al*. and Monaghan *et al*. containing high total iron oxide (>29wt pct) as shown in Figure 5(b).

By studying reduction of iron oxide in FeO rich slag, most investigators [16-24] proposed that the reaction was first order with respect to FeO concentration in the bulk slag, and was most likely controlled by FeO mass transfer in the slag. If this is the case, the apparent rate constant can be converted to a mass transfer coefficient for FeO in the slag as done by Woolley and Pal. [24] A

detailed explanation of this conversion is shown in the Appendix. Depending on the availability of required information to complete the conversion, apparent rate constants in some of those studies were converted and included in Figures 5(a) and (b), also listed in the appendix in Table AIV. When carbon dissolved from a graphite crucible was the reductant for FeO, Galgali *et al.* [17] found that the mass transfer coefficient of FeO decreased with increasing of FeO content in the slag. Although in the case of Murthy *et al.* [18] the apparent rate constant showed an increase, the converted k_{FeO} was found to decrease slightly with increasing FeO content. Apparently, a further detailed analysis of these last two studies is required in order to understand this discrepancy. The k_{FeO} in these cases were also listed in Table AIV, but have not been brought into this discussion. It is worth noting that other workers [22,24] have successfully correlated k_{FeO} with the rate of CO bubble generation to justify the effect of FeO content on k_{FeO}.

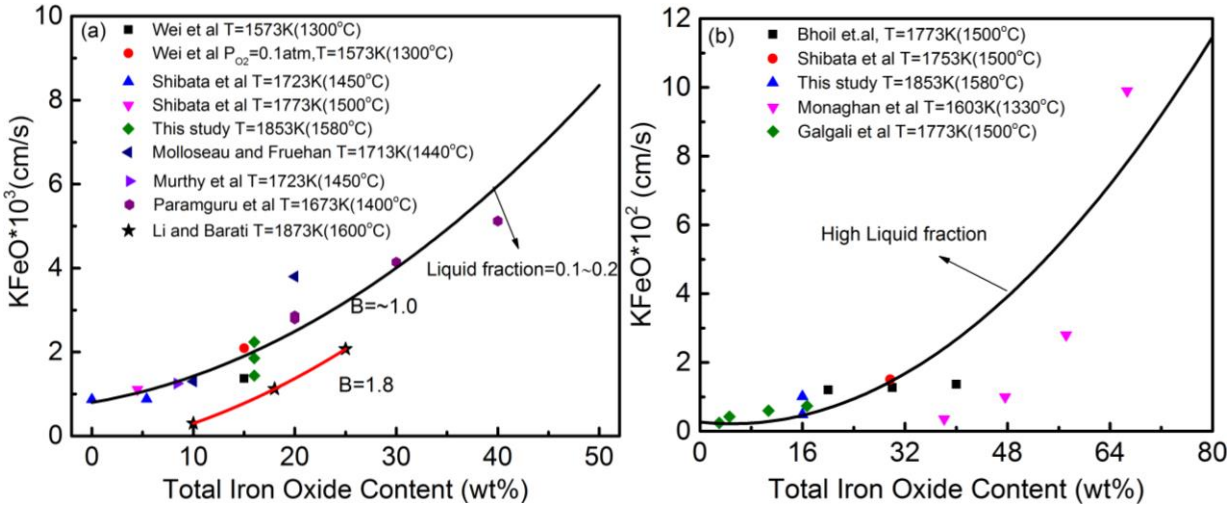

Fig. 5—k_{FeO} as a function of total iron content in the slag: (a) Low liquid fraction and (b) High Liquid fraction

All the data presented in Figure 5 show an excellent fit to a parabolic relationship between total iron oxide and the mass transport coefficient of FeO in the slag. Molloseau and Fruehan [7], B. Sarma [8] also observed a similar effect of FeO in the slag on mass transfer coefficient of FeO but did not offer a detailed explanation. From Figure 5, it is interesting to note that comparing data for high and low liquid fraction slags, they scale in reasonable approximation to the ratio of liquid fraction. It is also worth pointing that in Figure 5(a) although the k_{FeO} in the case of Li and Barati [16] follows a parabolic function, its' values are lower than other cases due to the higher slag basicity (B=1.8) slag compared to that (B=~1) employed in other studies. High basicity slag would increase the effective viscosity as shown by Li and Barati [16], which leads to a higher foam index [15] and lower liquid fraction.

In the current case we are expressing oxygen transfer as mass transport of FeO. However, it is more realistic to consider oxygen to be transported in the form of either O^{2-} or singly charged oxygen species hopping from site to site on silicate chains. Therefore the flux will require charge balancing either by concurrent transport of cations or by countercurrent transport of electrons.

Barati and Coley [25] demonstrated that at FeO contents of greater than 5%, electronic conduction via small polaron hopping was dominant and that the electronic conductivity was a parabolic function of total iron oxide content. Therefore, if in the current case, oxygen transport is controlled by the conduction of charge balancing electrons, the nominal mass transfer coefficient of FeO, k_{FeO} can be expected to follow a parabolic relationship with total iron in the slag. All the data in Figure 5 from different researchers under a wide ranged temperatures shows an excellent fit, which suggests that the effect of temperature on the $k_{FeO}$was relatively small. This observation is not consistent with the temperature effect on electronic conductivity observed by Barati and Coley [26]. Employing the Melts database in Factsage 6.4^{TM}, the activation energy of viscous flow for several cases in Figure 5 was estimated to have a magnitude of 100 kJ/mol. This estimation indicates that the temperature might have a larger effect on mass transfer coefficient than implied by Figure 5. At present the authors cannot offer a definitive explanation for this discrepancy.

B. Dynamic Interfacial Oxygen Potential

Knowing k_{FeO} in the slag, the interfacial oxygen potential between bloated metal droplets and slag can be calculated based on Eq. 2. According to the results in Table II, mass transfer of FeO in dense slag is more than four times faster than in foamy slag. In the present work, dephosphorization was mostly complete before droplets entered the foamy slag. Therefore, only the P_{O2}^{i} at the initial stage before the metal droplet completely enters the foamy slag, was calculated. As examples of the range of droplet behavior observed in the current work, the dynamic interfacial oxygen potential was calculated for droplets with 0.007, 0.014 and 0.021 wt pctS.

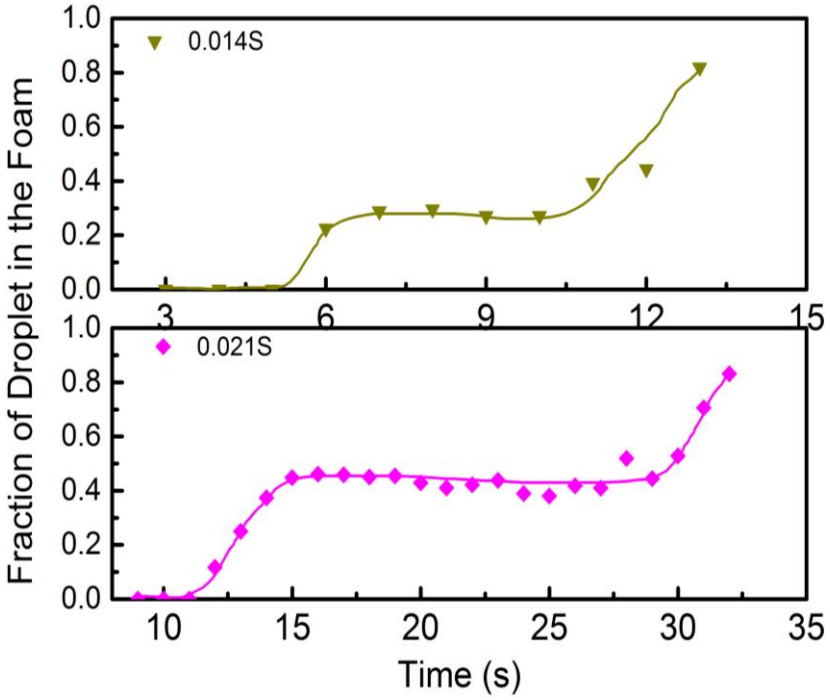

Fig. 6—Fraction of droplet surface area in the foam as a function of time.

To account for periods in which droplets sit between the foamy slag and dense slag, the changing fraction of droplet surface area in the foamy slag was measured and plotted in Figure 6 for droplets with 0.014 and 0.021wt pctS. After approximately 5 seconds, 0.014wt pctS droplets start to float up into the foamy slag, while 0.021wt pctS droplets begin to float up after around 12 seconds due to their longer incubation time for swelling. The mass transfer coefficient k_{FeO} used to calculate the interfacial oxygen potential was calculated as an average of foamy slag and dense slag weighted according to the fraction of the droplet surface exposed to each.

Based on Eq. 2, the dynamic interfacial oxygen potential for droplets before rising entirely into the foamy slag was calculated and is shown in Figure 7.

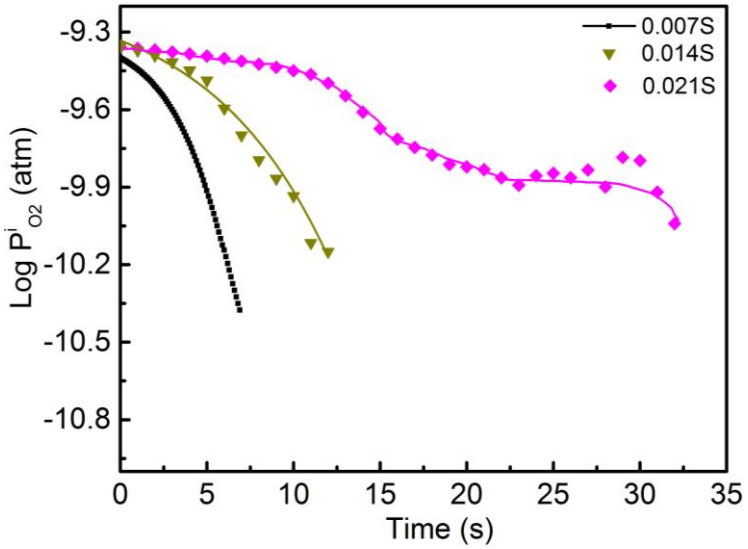

Fig. 7—The dynamic interfacial oxygen potential between bloated droplets and slag.

This shows that P_{O2}^{i} for all the cases decreases as reaction proceeds but the rate of decrease varies with the decarburization rate and incubation time. For droplets with lower sulfur content (0.007 and 0.014wt pct), the P_{O2}^{i} drops very rapidly because their short incubation times leading to an early entry into the foamy slag which has a low mass transfer coefficient for FeO and also the low liquid volume becomes depleted of FeO. While for droplets with 0.021wt pctS, P_{O2}^{i} decreases much more slowly because of the lower decarburization rate coupled with the longer incubation period which causes them to remain in the dense slag with a higher mass transfer coefficient for FeO and greater reservoir of FeO.

One would assume that in a real BOF the droplets would be subject to the k_{FeO} of a foamy slag but that FeO would not be depleted because of constant replenishing via reaction with the oxygen jet.

C. The Effect of Dynamic Interfacial Oxygen Potential on Dephosphorization Kinetics

It is well established that the balance between control by mass transfer in the slag and by mass transfer in the metal is heavily influenced by the phosphorus partition ratio; a significant change

in L_P causes a shift in reaction mechanism from one controlling step to another. [2, 4-5] By knowing the dynamic P_{O2}^{i} the phosphorus partition ratio L_P and the overall mass transfer coefficient k_o can be calculated as a function of time based on Eq. 3 and 5:

$$k_o = \frac{1}{\frac{\rho_m}{k_s \rho_s L_P} + \frac{1}{k_m}} \quad [5]$$

where k_s and k_m are mass transfer coefficient in slag and metal phase, respectively.

Figure 8 shows the phosphorous partition ratio and the overall mass transfer coefficient as a function of time for bloated droplets in the current study, calculated based on the dynamic interfacial oxygen potential. Here, k_s and k_m were chosen to be 0.01 and 0.085cm/s based on analysis of dephosphorization presented in a previous publication by the authors. [5]

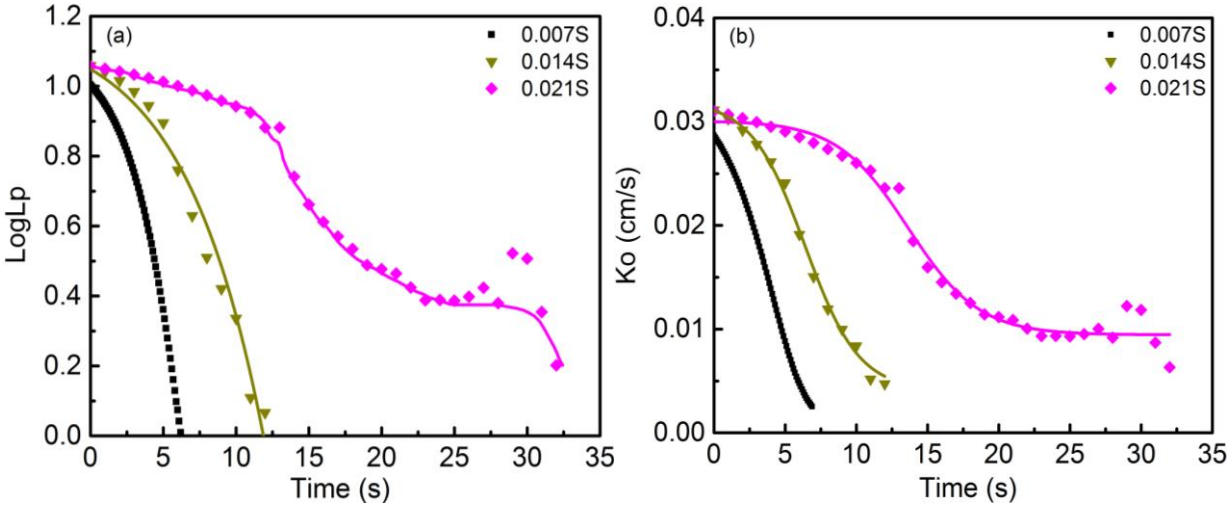

Fig. 8—(a) Phosphorus partition ratio (L_P) and (b) overall mass transfer coefficient (k_o) as a function of time for the study of bloated droplets

Figure 8(a) shows that the driving force for dephosphorization, L_P, decreases with time due to the decreasing interfacial oxygen potential as reduction of FeO from the slag proceeds. Figure 8(b) presents the change of overall mass transfer coefficient during the dephosphorization period shown in Figure 2. It shows that the controlling step for dephosphorization of bloated droplets in the current study is initially mixed control by mass transport in both the metal and slag. And the value of $k_o$is 0.03cm/s. As phosphorus partition ratio decreases, the rate determining step shifts to mass transport in slag with a value of k_o less than 0.01cm/s. The changes in k_o with time agree very well with the authors' previous observations of dephosphorization kinetics. [5]

Shibata *et al.* [4] conducted a similar analysis of mixed control to that presented above, however these workers presented their data as resistance to mass transfer rather than an overall mass transfer coefficient. To facilitate comparison Shibata's data analysed in terms of k_o is presented in Figure 9. These workers reported k_s and k_m to be 0.013 and 0.021cm/s. Using these values, the determined L_P and k_o are shown in Figure 9. The trends presented in Figure 9 are exactly the same

as those found in the current authors' research, although the overall mass transfer coefficient is relatively lower. Deeper analysis shows that the source of the discrepancy lies in the current case having a significantly higher mass transfer coefficient for phosphorus in the metal. The authors are not able to offer a definitive explanation for this discrepancy but believe it must be related to the way in which CO gas stirs the metal. It is worth noting that in the current case CO nucleated throughout the droplet.

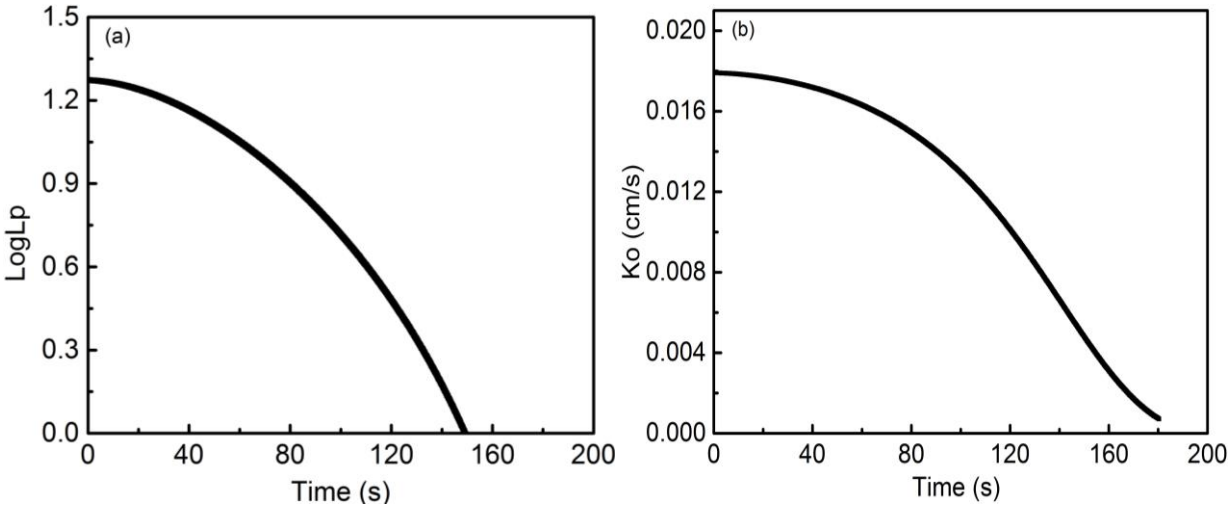

Fig. 9—(a) L_P and (b) k_o as a function of time for the slag in Shibata's work.

The relative contribution of the metal phase to the overall resistance to mass transport was determined by Shibata *et al.* to be 95 pct at the beginning of the reaction decreasing to 30 pct towards the end of the reaction. The relatively greater fraction of control by mass transport in the metal when compared with the current work can be explained by less depletion of FeO in the slag in the case of Shibata *et al*. and by a lower mass transfer coefficient in the metal.

From above discussion, the rate controlling step of dephosphorization is dependent on the decarburization behavior of metal droplets. The prediction of rate determining step using the model developed in the current study showed very reasonable agreement with other researchers' work. [2-4] Therefore, it is worth examining how the decarburization rate might affect the rate controlling step in real steelmaking conditions. Assuming metal droplets under typical steelmaking conditions have similar decarburization behavior to droplets with 0.014wt pctS in this study, and choosing reasonable mass transfer coefficients for slag (0.005cm/s) and metal (0.06cm/s) based on the above discussion, the relationship between overall mass transfer coefficient k_o and the decarburization rate has been evaluated using the above model. In this calculation, the slag composition was chosen to be 45wt pctCaO-20wt pctSiO_2-15wt pctFeO-10wt pctMnO-5wt pctMgO based on typical industrial data during the middle blow stage in the BOF. [27] The calculated result is shown in Figure 10. The two vertical dotted lines represent the range of decarburization rate observed in this study at 1853K(1580ºC). The corresponding L_P for a steelmaking slag will be between 380 and 900. This figure shows that under steelmaking conditions dephosphorization of metal droplets in the emulsion zone is more likely to be limited by the mass transport in the metal phase. This finding

is reasonable under steelmaking conditions if one considers the high basicity of slag and no depletion of FeO in the slag.

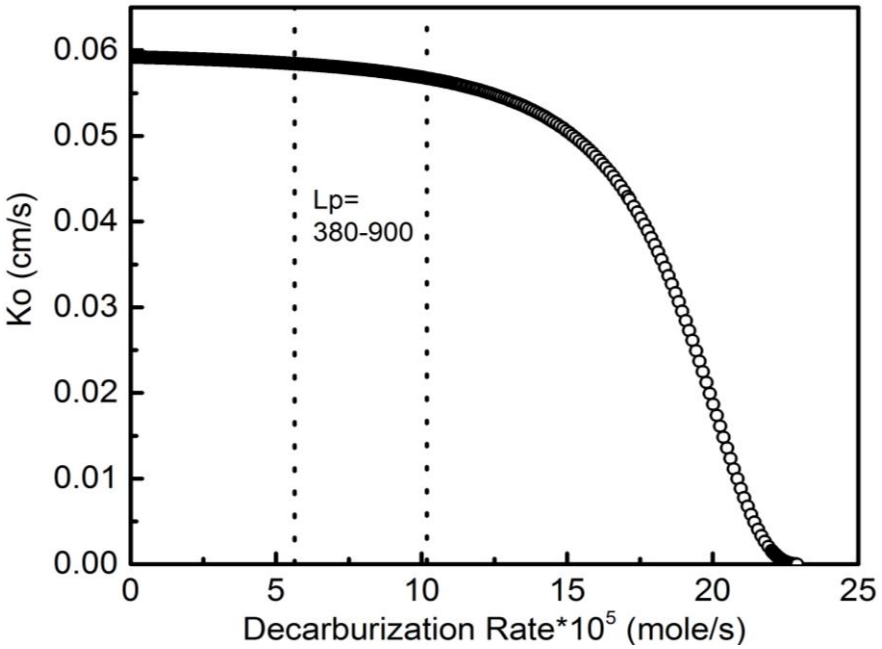

Fig. 10—The effect of decarburization rate on overall mass transfer coefficient.

V. Conclusion

The dynamic interfacial oxygen potential between bloated droplets and slag was determined using the phosphorus partition ratio at the reversion point. Analysis of this data by considering the balance between oxygen supply from oxidizers in the slag and oxygen consumption by alloy elements in the metal allowed the mass transfer coefficient of "FeO" to be determined. The mass transfer coefficient was found to show a parabolic increase with total iron oxide in the slag. The calculated results also showed that the mass transfer of FeO in dense slag was much faster than in foamy slag. Knowing the mass transfer coefficient for FeO and the decarburization rate of the droplet allows the dynamic interfacial oxygen potential to be calculated at any time during the reaction. From this study, the following conclusions can be drawn.

1. When the mass transfer of oxygen in the slag is represented as mass transfer of "FeO", the mass transfer coefficient shows a parabolic correlation with total iron oxide in the slag and is not strongly dependent on temperature. This is consistent with transport controlled by charge balancing by small polaron hopping via an Fe^{3+}/Fe^{2+} couple.

2. The mass transfer coefficient of FeO in the dense slag shows a strong linear correlation with the liquid fraction in foamy slag due to transport pathways being limited to the liquid portion.

3. Calculations predict that the rate determining step for dephosphorization of bloated droplets in laboratory studies, shifts from mass transport in both metal and slag to mass transport in slag.

This is caused by a decrease in the dynamic interfacial oxygen potential with time because of FeO depletion.

4. Contrary to most laboratory studies, the calculation method adopted in the current study shows that dephosphorization of metal droplets in the emulsion zone under real steelmaking conditions will be limited by mass transport in the metal phase because of the high basicity of the slag and the fact that FeO is continuously replenished.

ACKNOWLEDGEMENTS

The authors thank member companies of McMaster Steel Research Centre and the Natural Science and Engineering Research Council of Canada (NSERC) for funding this project.

REFERENCES

1. S. Ohguchi, D. G. C. Robertson, B. Deo, P. Grieveson and J. H. E. Jeffes: *Ironmak. Steelmak.*, 1984, vol. 11, pp. 202-13.
2. P. Wei, M. Ohya, M. Hirasawa, M. Sano and K. Mori: *ISIJ Int.*, 1993, vol. 33 (8), pp. 847-54.
3. B. J. Monaghan, R.J. Pomfret, and K.S. Coley: *Metall. Trans. B*, 1998, vol. 29B, pp. 111-18.
4. E. Shibata, H. Sun and K. Mori: *Metall. Trans. B*, 1999, vol. 30B, pp. 279-86.
5. K. Gu, N. Dogan and K. Coley: *Metall. Trans. B*, DOI: 10.1007/s11663-017-1002-0.
6. E. Chen and K. Coley: *Ironmak. Steelmak.*, 2010, vol. 37 (7), pp. 541-45.
7. H. Sun: *ISIJ Int.*, 1993, vol. 33 (11), 1560-69.
8. T. Mori: *Trans. Jpn. Inst. Met.*, 1984, vol. 25 (11), pp. 761-71.
9. C. L. Molloseau and R. J. Fruehan: *Metall. Trans. B*, 2002, vol. 33B, pp. 335-44.
10. B. Sarma: PhD Thesis, Carnegie Mellon University, Pittsburgh, PA, 1992, pp. 30-31 and 149.
11. D. J. Min and R. J. Fruehan: *Metall. Trans. B*, 1992, vol. 23B, pp. 29-37.
12. P. Wei, M. Sano, M. Hirasawa, and K. Mori: *ISIJ Int.*, 1993, vol. 33, 479-87.
13. H. Gou, G. A. Irons, and W. Lu: *Metall. Trans. B*, 1996, vol. 27B, pp. 79-88.
14. T. Zhu, M. P. King, K. S. Coley and G. A. Irons: *Metall. Trans. B*, 2012, vol. 43B, pp. 31-36.
15. S. Jung and R. J. Fruehan: *ISIJ Int.*, 2000, vol. 40 (4), pp. 348-55.
16. J. Li and M. Barati: *Metall. Trans. B*, 2009, vol. 40B, pp. 17-24.
17. R. K. Galgali, P. Datta, A. K. Ray, K. K. Prasad and H. S. Ray: *Ironmak. Steelmak.*, 2001, vol. 28 (4), pp. 321-28.
18. G. G. Krishna Murthy, Y. Sawada and J. F. Elliot: *Ironmak. Steelmak.*, 1993, vol. 20 (3), pp. 179-190.
19. G. G. Krishna Murthy, A. Hasham and U. B. Pal: *ISIJ Int.*, 1994, vol. 34 (5), 408-13.
20. R. K. Paramguru, H. S. Ray and P. Basu: *Ironmaking and Steelmaking*, 1996, vol. 23 (4), pp. 328-34.
21. R. K. Paramguru, H. S. Ray and P. Basu: *ISIJ Int.*, 1997, vol. 37 (8), 756-761.
22. R. K. Paramguru, R. K. Galgali and H. S. Ray: *Metall. Trans. B*, 1997, vol. 28B, pp. 805-10.
23. B. Bhoi, A. K. Jouhari, H. S. Ray and V. N. Misra: *Ironmak. Steelmak.*, 2006, vol. 33 (3), pp. 245-52.
24. D. E. Woolley and U. B. Pal: *ISIJ Int.*, 1999, vol. 39 (2), 103-12.
25. M. Barati and K. Coley: *Metall. Trans. B*, 2006, vol. 37B, pp. 51-60.
26. M. Barati and K. Coley: *Metall. Trans. B*, 2006, vol. 37B, pp. 41-49.
27. C. Cicutti, M. Valdez, T. Perez, R. Donayo and J. Petroni: *Latin Am. Appl. Res.*, 2002, vol. 32, pp. 237-240.
28. M. Hino and K. Ito: *Thermodynamic Data for Steelmaking*, Tohoku University Press, Sendai. 2009, pp. 259-64.
29. S. Basu, A.K. Lahiri and S. Seetharaman: *Metall. Trans. B*, 2008, vol. 39B, pp. 447-56.

APPENDIX

A-1 Derivation of Equation [2].

The derivation of Eq. [2] from Eq. [1] can be demonstrated as follows:

$$k_{FeO}\left(C_{FeO}^{b}-C_{FeO}^{i}\right)=\frac{1}{A}\frac{dn_{CO}}{dt} \quad [1]$$

where C_{FeO}^{b} is the instantaneous concentration of FeO in the bulk slag at any given time t, which can be calculated via Eq. [A1] by knowing the amount of FeO (n_{FeO}) has been reduced, *i.e.*, the amount of CO gas (n_{CO}) generated at time t.

$$C_{FeO}^{b}=C_{FeO}^{o}-\frac{1}{V_S}n_{FeO}=C_{FeO}^{o}-\frac{1}{V_S}\int_{n_{CO},t=0}^{n_{CO},t=t}dn_{CO} \quad [A1]$$

Substituting C_{FeO}^{b} into Eq. [1], one can obtain the concentration of FeO at the slag-metal interface.

$$C_{FeO}^{i}=C_{FeO}^{o}-\frac{1}{V_S}\int_{n_{CO},t=0}^{n_{CO},t=t}dn_{CO}-\frac{1}{A}\frac{1}{k_{FeO}}\frac{dn_{CO}}{dt} \quad [A2]$$

The equilibrium constant for dissociation of FeO at the interface can be expressed as,

$$K_{Fe}=\frac{a_{Fe}^{i}a_{O}^{i}}{\gamma_{FeO}X_{FeO}^{i}} \quad [A3]$$

Knowing the overall molar density of slag C_s, X_{FeO}^{i} can be expressed as $\frac{C_{FeO}^{i}}{C_s}$. Then a_O^i can be written as Eq. [A4] by rearranging Eq. [A3],

$$a_{O}^{i}=\frac{\gamma_{FeO}K_{Fe}}{C_s a_{Fe}^{i}}C_{FeO}^{i} \quad [A4]$$

Substituting Eq. [A2] into Eq. [A4], one can obtain,

$$a_{O}^{i}=\frac{\gamma_{FeO}K_{Fe}}{C_s a_{Fe}^{i}}\left(C_{FeO}^{o}-\frac{1}{V_S}\int_{n_{CO},t=0}^{n_{CO},t=t}dn_{CO}-\frac{1}{A}\frac{1}{k_{FeO}}\frac{dn_{CO}}{dt}\right) \quad [A5]$$

Considering the dissolution of oxygen into metal phase with the following reaction constant,

$$K_O=\frac{a_O^i}{{P^i}_{O_2}^{1/2}}\Rightarrow {P^i}_{O_2}^{1/2}=\frac{a_O^i}{K_O} \quad [A6]$$

the expression for calculating oxygen potential (equivalent oxygen partial pressure) at the slag-metal interface can be expressed as Eq. [2] finally.

$$P_{O2}^{i}=\left[\frac{\gamma_{FeO}K_{Fe}}{C_s * a_{Fe}^{i} * K_O}\left(C_{FeO}^{o}-\frac{1}{V_S}\int_{n_{CO},t=0}^{n_{CO},t=t}dn_{CO}-\frac{1}{A}\frac{1}{k_{FeO}}\frac{dn_{CO}}{dt}\right)\right]^2 \quad [2]$$

A-2 Calculation of Void Fraction

Assuming a constant cross-sectional area for the crucible, the volume of the slag may be represented by its depth. The initial slag height h_o, the dense slag depth h_{dense} and the depth of foaming slag h_{foam} at any given time can be measured via the recorded X-ray video. Then the liquid fraction of slag in the foam was calculated based on the Eq. [A7].

$$F_{liquid} = \frac{h_o - h_{dense}}{h_{foam}} \quad [A7]$$

Then the void fraction $= 1 - F_{liquid}$.

For droplets with 0.014 and 0.021wt pctS, which go through phosphorus reversion while sitting between the dense slag and foaming slag as shown in Figure 3, the liquid fraction F^*_{liquid} of the slag in contact with the droplet was represented by a weighted average of foamy and dense slag in proportion to their contact with the droplet, *i.e.*,

$$F^*_{liquid} = \frac{V_{droplet\ in\ the\ foam}}{V_{droplet}} F_{liquid1} + \frac{V_{droplet\ in\ dense\ slag}}{V_{droplet}} F_{liquid2} \quad [A8]$$

where $V_{droplet}$, $V_{droplet\ in\ the\ foam}$ and $V_{droplet\ in\ dense\ slag}$ are total droplet volume, the partial volume of droplet in foaming slag and dense slag, respectively. $F_{liquid1}$ is the slag liquid fraction obtained from Eq. A-7, while $F_{liquid2}$ represents the liquid fraction of dense slag and is one.

The related reactions and their reaction equilibrium constants were listed in Table AI: [28]

Table AI: Reactions and Their Equilibrium Constants used in This Study

Reactions	Reaction Constant
$(FeO) = [Fe] + [O]$ (1)	$\log K_1 = \frac{-6372}{T} + 2.73$
$[C] + [O] = CO$ (2)	$\log K_2 = \frac{1160}{T} + 2.003$
$\frac{1}{2}(O_2)_{gas} = [O]$ (3)	$\log K_3 = \frac{6120}{T} + 0.18$
$MnO = [Mn] + [O]$ (4)	$\log K_4 = \frac{-15046.6}{T} + 6.70$
$\frac{1}{2}(P_2)_{gas} = [P]$ (5)	$\log K_P = \frac{8240}{T} - 0.28$

In this study, the empirical equation developed by Basu *et al.* [29] was also used to estimate γ_{FeO}.

$$\log \gamma_{FeO} = -0.7335 \times \log X_{FeO} - 0.2899$$

Slag and metal compositions taken from the work of Shibata *et al.* [4] and from Wei *et al.* [2] are given in Tables AII and AIII. These data are employed to calculate k_{FeO} and P^i_{O2} below.

Table AII: Slag Compositions (wt pct)

Slag	MnO	FeO	CaO	SiO_2	CaF_2	Li_2O
Shibata *et al.* (A-1)	_	29.7	29.4	32.1	8.8	
Shibata *et al.* (B-12)	22.4	4.5	30.3	33.3	9.5	
Shibata *et al.* (C-1)	39.6	5.4	22.0	23.8	9.2	
Shibata *et al.* (K-5)	36.7	_	27.6	27.0	8.8	
Wei *et al.*	15(FetO)		32.6	35		17.4

Table AIII: Experimental Conditions and Initial Metal Compositions (wt pct)

Number	Temperature K(°C)	C	P	Si	Mn	S
Shibata *et al.* (A-1)	1773(1500)	3.72	0.089	0.187	_	_
Shibata *et al.* (B-12)	1773(1500)	3.81	0.092	0.194	0.015	_
Shibata *et al.* (C-1)	1723(1450)	3.79	0.102	0.215	0.010	_
Shibata *et al.* (K-5)	1723(1450)	3.80	0.096	0.167	0.020	0.098
Wei *et al.* (P_{O2}=0atm)	1573(1300)	4.44	0.1			
Wei *et al.* (P_{O2}=0.1atm)	1573(1300)	4.18	0.044			

A-3 Dynamic Interfacial Oxygen Potential

The equations employed in calculating $P_{O_2}^i$ for the four cases taken from the work of Shibata *et al.* [4] and Wei *et al.* [2] listed in Table AII and AIII were as follows:

A-1 slag:

$$P_{O2}^i = \left[\frac{\gamma_{FeO}K_1}{C_s * a_{Fe}^i * K_3}\left(C_{FeO}^o - \frac{1}{V_s}\left(\int_{n_C,t=initial}^{n_C,t=t} dn_C + 2\int_{n_{Si},t=initial}^{n_{Si},t=t} dn_{Si}\right) - \frac{1}{A}\frac{1}{k_{FeO}}\left(\frac{dn_C}{dt} + 2\frac{dn_{Si}}{dt}\right)\right)\right]^2 \quad [A9]$$

K-5 slag:

$$P_{O2}^i = \left[\frac{\gamma_{MnO}K_4}{C_s * a_{Mn}^i * K_3}\left(C_{MnO}^o - \frac{1}{V_s}\left(\int_{n_C,t=initial}^{n_C,t=t} dn_C + 2\int_{n_{Si},t=initial}^{n_{Si},t=t} dn_{Si}\right) - \frac{1}{A}\frac{1}{k_{MnO}}\left(\frac{dn_C}{dt} + 2\frac{dn_{Si}}{dt}\right)\right)\right]^2 \quad [A10]$$

Eq. [A9] was developed by balancing the flux of FeO to the interface with the oxidation of carbon and silicon in the metal. Eq. [A10] was developed in the same way replacing FeO flux with that of MnO. Eq. [A11] applied the same logic but assumed oxygen supply by simultaneous flux of FeO and MnO and that Mn/MnO and Fe/FeO at the interface were in equilibrium with the same oxygen potential. Similarly, Eq. [A12] was developed by balancing the flux of FeO to the interface with the oxidation of carbon in the metal. Wei *et al.* defined the iron oxide in their slag as Fe_tO in

recognition that some of the iron was present as Fe^{3+}, however for simplicity of calculation it has been assumed that the iron oxide was in the form of FeO.

B-12 and C-1 slag:

$$P_{O2}^{i}=\left[\frac{1}{\left(\frac{C_S*a_{Fe}^{i}*k_{FeO}}{\gamma_{FeO}*K_1}+\frac{C_S*a_{Mn}^{i}*k_{MnO}}{\gamma_{MnO}*K_4}\right)*K_3}\left[\left(k_{FeO}+\frac{k_{MnO}*\gamma_{FeO}*K_{1*}a_{Mn}^{i}*K_4}{a_{Fe}^{i}*\gamma_{MnO}}\right)*\left(C_{FeO}^{o}-\frac{1}{V_s}\left(\int_{n_C,t=initial}^{n_C,t=t}dn_C+2\int_{n_{Si},t=initial}^{n_{Si},t=t}dn_{Si}\right)\right)-\frac{1}{A}\left(\frac{dn_C}{dt}+2\frac{dn_{Si}}{dt}\right)\right]\right]^2 \quad [A11]$$

Fe_tO slag:

$$P_{O2}^{i}=\left[\frac{\gamma_{FeO}K_1}{C_S*a_{Fe}^{i}*K_3}\left(C_{FeO}^{o}-\frac{1}{V_s}\int_{n_C,t=initial}^{n_C,t=t}dn_C-\frac{1}{A}\frac{1}{k_{FeO}}\frac{dn_C}{dt}\right)\right]^2 \quad [A12]$$

where γ is the Raoult's activity coefficient of oxides in the slag at the interface and calculated the empirical equation developed by Basu *et al.* [29] and regular solution model, α^i represents the Henrian activity in liquid metal at the interface and obtained based on interaction coefficients for different solutes.[17] K is the equilibrium constant for reactions listed in Table AIV, C_s and C^o are molar density of slag and initial concentration of oxides, respectively. V_s represents the volume of slag, $\frac{d_n}{dt}$ is the reaction rate (mole/s) for Si and C which is determined empirically using experimental data.

A-4 Mass Transfer Coefficient k_{FeO} Conversion.

If the reduction of iron oxide in FeO rich slag follows first order reaction kinetics with respect to FeO in the bulk slag phase and is controlled by the mass transfer of FeO in the slag, the rate expression may be given as follows:

$$r_{FeO}=k(\%FeO)_{bulk\ slag} \quad [A13]$$

where r_{FeO} is reaction rate with the unit of $(pct\ FeO)*s^{-1}$and also equal to the reaction rate in terms of CO, *i.e.*, r_{CO}; $k$is the rate constant and has a unit of s^{-1}or min^{-1}. It is well known that the first order reaction rate can also be written as:

$$r_{FeO}=k_{FeO}\frac{A}{V}(\%FeO)_{bulk\ slag}=k_{FeO}\frac{A}{Ah_o}(\%FeO)_{bulk\ slag}=\frac{k_{FeO}}{h_o}(\%FeO)_{bulk\ slag} \quad [A14]$$

where $k_{FeO}$is mass transfer coefficient of FeO, V represents slag volume in this case, A is the area of slag-metal interface and normally treated as cross-sectional area of crucible, h_o represents the slag height.

Then we are able to convert the rate constant (with unit of s^{-1}) in Eq. [A13] to k_{FeO} via the following expression;

$$k = \frac{k_{FeO}}{h_o} \quad [A15]$$

Some authors expressed the reaction rate as in Eq. [A16] with the unit of $\text{mol} \times cm^{-2} \times s^{-1}$,

$$r_{FeO} = J_{FeO} = k_{FeO} C_{FeO\,bulk\ slag} = k_{FeO} \frac{\rho_s}{100 M_{FeO}} (\%FeO)_{bulk\ slag} \quad [A16]$$

where $\rho_s$is the density of slag ($g \times cm^{-3}$), M_{FeO} represents the molecular weight of FeO. Then Eq. [A13] can be rewritten as:

$$r_{FeO} = k'(\%FeO)_{bulk\ slag}$$

Similarly, r_{FeO} is reaction rate but with the unit of $\text{mol} \times cm^{-2} \times s^{-1}$and $k' = k_{FeO} \frac{\rho_s}{100 M_{FeO}}$ is the rate constant with the unit of $\text{mol} \times cm^{-2} \times s^{-1}(pct\ FeO)^{-1}$. Therefore, k' can be converted to k_{FeO} based on Eq. [A16].

Table AIV: Converted k_{FeO} from Rate Constants Determined by Different Researchers

Investigator	T/(K(°C))	B	Fe_tO/(wt pct)	$k' \times 10^7/(\text{mol} \times cm^{-2} \times s^{-1}(pct\ FeO)^{-1})$	$k \times 10^3(s^{-1})$	$k_{FeO} \times 10^3$(cm/s)
Li and Barati.	1873(1600)	1.8	10	1.1		0.30
Li and Barati.	1873(1600)	1.8	18	4.1		1.12
Li and Barati.	1873(1600)	1.8	25	7.6		2.07
Paramguru *et al*.	1673(1400)	1	20		1.58	2.79
Paramguru *et al*.	1673(1400)	1	20		1.62	2.86
Paramguru *et al*.	1673(1400)	1	30		2.45	4.14
Paramguru *et al*.	1673 (1400)	1	40		3.16	5.12
Bhoil *et al*.	1873 (1600)	1	20		3.33	12.0
Bhoil *et al*.	1873 (1600)	1	30		3.53	12.7
Bhoil *et al*.	1873 (1600)	1	40		3.80	13.7
Galgali *et al*.	1773(1500)	1.2	3.0		0.82	2.45
Galgali *et al*.	1773(1500)	1.2	4.6		1.42	4.26
Galgali *et al*.	1773(1500)	1.2	10.7		2.0	6.0
Galgali *et al*.	1773(1500)	1.2	16.4		2.45	7.35
Galgali *et al*.	1773(1500)*	1.2	5			3.78
Galgali *et al*.	1773(1500) *	1.2	10			3.80
Galgali *et al*.	1773(1500) *	1.2	15			2.90
Galgali *et al*.	1773(1500) *	1.2	20			2.36
Murthy *et al*.	1723(1450) $^{\Delta}$	1.1	8.4		4.31	1.25$^{\Delta}$
				$k \times 10^5/(\text{mol} \times cm^{-2} \times s^{-1})$		
Murthy *et al*.	1823(1550) *	1.1	5.5	1.4		6.62
Murthy *et al*.	1823(1550) *	1.1	8.4	1.88		5.74
Murthy *et al*.	1823(1550) *	1.1	13.2	2.05		3.89
Murthy *et al*.	1823(1550) *	1.1	18	2.6		3.55

$^{\Delta}$This value of mass transfer coefficient is the mean value for slag with constant FeO content but different slag weights. *Those values were not brought into the discussion of Figure 5.